Computational Materials Science 166 (2019) 311–317

Contents lists available at ScienceDirect

Computational Materials Science

journal homepage: www.elsevier.com/locate/commatsci

Thermodynamic analysis and atomistic modeling of subsurface cavitation in photomechanical spallation

Maxim V. Shugaev, Leonid V. Zhigilei*

Department of Materials Science and Engineering, University of Virginia, 395 McCormik Road, Charlottesville, VA 22904-4745, USA

ARTICLE INFO

Keywords:
Cavitation
Photomechanical spallation
Laser-materials interactions
Subsurface voids
Molecular dynamics simulations

ABSTRACT

The thermodynamic conditions defining the spatial extent of a subsurface region affected by the nucleation and growth of voids in photomechanical spallation of metals is investigated theoretically and in atomistic simulations. A theoretical analysis of cavitation in a surface region of a target melted by laser irradiation suggests a functional form for the temperature dependence of the cavitation threshold. A series of small-scale molecular dynamics simulations performed for Al, Ag, Cr, and Ni has revealed the minimum value of the free energy barrier that results in the onset of cavitation on the timescale of 10s of ps, which is a typical duration of transient tensile stresses produced by the unloading wave generated in the spallation regime. The predictive ability of the theoretical description is verified in large-scale simulations of photomechanical spallation of a Ni target and ablation of an Al target in the phase explosion regime. The temporal and spatial evolution of the free energy barrier for the onset of cavitation under conditions of short pulse laser processing is shown to univocally define the region where the nucleation of voids takes place.

1. Introduction

Short (femtosecond and picosecond) pulse laser processing and ablation of metal targets is widely used in modern applications [1–8] and provides unique capabilities for modification of material properties and surface morphology [7–16]. Dynamic relaxation of laser induced stresses, which are particularly high in the regime of stress confinement [17–19], can result in the generation of a tensile unloading wave that, in turn, can lead to the nucleation of voids in the molten surface region of the target. The voids can subsequently collapse, be trapped by the resolidification process leading to surface swelling [16,20,21], or grow and coalesce leading to photomechanical spallation, *i.e.*, complete separation and removal of the liquid layer [17–19]. Although these processes have been extensively studied in large-scale atomistic simulations [16,18,19,22–29], realistic description of the spallation process in continuum-level models remains challenging and requires special consideration. The onset of sub-surface cavitation in one-dimensional (1D) hydrodynamics simulations of laser spallation has been treated using the classical nucleation theory [30], as well as with Grady's criterion [31] for spallation threshold based on the energy cost of void growth during the time of tensile loading [21]. The 1D nature of the models, however, makes it difficult to provide an adequate description of the initial stage of void nucleation and growth.

Theoretical analysis based on the classical nucleation theory and atomistic modeling have provided important insights into conditions leading to the onset of the cavitation in an overstretched liquid and enabled estimations of the cavitation threshold and void nucleation rate [32–39]. Most of the atomistic simulations, however, are performed for systems described by Lennard-Jones interatomic potential, which is unable to accurately describe the behavior and properties of molten metals. Moreover, the temperature dependence of the cavitation threshold is neglected in most of these studies, which are performed under conditions of constant temperature and constant total volume. Meanwhile, short pulse laser irradiation produces strong temperature and pressure gradients and rapidly changing thermo-mechanical conditions in the surface region of the irradiated target [24], which cannot be approximated without considering the temperature dependence of the cavitation threshold. In this paper, we suggest a criterion for the onset of cavitation in a molten metal that accounts for the temperature dependence of relevant thermodynamic parameters. The criterion is suitable for predicting the location and size of the subsurface region affected by laser-induced cavitation as well as the amount of spalled material. The analytical description is parametrized based on the results of atomistic simulations and verified against the predictions of large-scale molecular dynamics (MD) simulations of laser spallation and phase explosion.

* Corresponding author.
E-mail address: lz2n@virginia.edu (L.V. Zhigilei).

https://doi.org/10.1016/j.commatsci.2019.05.017
Received 9 February 2019; Received in revised form 4 May 2019; Accepted 8 May 2019

2. Criterion for the onset of cavitation

The free energy change due to appearance of a spherical cavity of radius r in a system under tension can be expressed as:

$$\Delta G = \frac{4\pi r^3}{3}P + 4\pi r^2\sigma, \quad (1)$$

where P and σ are the pressure in the system and the surface tension of liquid-vapor interface, respectively. Since the magnitude of pressure variation in a target irradiated under conditions of stress confinement is usually much larger than the saturated vapor pressure, P_v, in a wide range of temperatures above the melting point of a target material, the contribution of the vapor pressure is neglected here to simplify the analysis. Thus, we consider the regime of photomechanical spallation, when the dominant driving force responsible for the appearance of the voids or cavities is the dynamic relaxation of the laser-induced stresses (see Ref. [18] for the discussion of the terminology used for the description of this process). As the temperature approaches the critical point, however, $P - P_v$ should be used in the free energy equation instead of P, and the release of the vapor phase can drive the massive nucleation and growth of the vapor bubbles even in the absence of any negative/tensile pressure. The conditions when the release of the vapor phase starts to make the dominant contribution to the material decomposition and ejection correspond to the transition from spallation to phase explosion or explosive boiling.

For a spherical cavity generated in the regime of photomechanical spallation, the critical radius and free energy barrier for the onset of the cavitation can be obtained from Eq. (1) using a condition of $d(\Delta G)/dr|_{r_c} = 0$, which yields $r_c = -2\sigma/P$ and $G_0 = \Delta G(R_c) = 16\pi\sigma^3/3P^2$ [32–39]. For a system under tension ($P < 0$), the rate of void nucleation can then be written as:

$$R = R_0 \times exp(-G_0/k_BT) = R_0 \times exp(-16\pi\sigma^3/3P^2k_BT), \quad (2)$$

where k_B and T are Boltzmann constant and temperature. The prefactor R_0 is expressed in units of nuclei per second per cubic meter and can be estimated as $R_0 \approx k_BT/hV_a$ [36], where V_a is the atomic volume, and h is Planck's constant. For a typical metal, this estimation yields R_0 on the order of 10^{42} [$s^{-1}\,m^{-3}$], and a more accurate consideration of the prefactor accounting for the number of surface atoms in the critical nucleus [36] increases R_0 up to $10^{44}\,s^{-1}\,m^{-3}$.

According to a large-scale atomistic simulations of laser-induced spallation of Ag and Al targets [16,24], the propagation of the unloading tensile wave through a molten parts of the targets generates approximately 100 voids within a volume of about $100 \times 100 \times 50\,nm^3$ during a time of about 20 ps, which suggests a nucleation rate of $R \sim 10^{34}\,s^{-1}\,m^{-3}$. By matching this rate in Eq. (2), a criterion for evaluation of the temperature dependence of the threshold tensile pressure for the onset of cavitation in short pulse laser spallation can be formulated:

$$P_{th}^2 = \frac{\alpha\sigma(T)^3}{k_BT}, \quad (3)$$

where $\alpha = 16\pi/3ln(R_0/R) \approx 0.7$ is obtained based on the estimation of the prefactor discussed above, $R_0 \sim 10^{44}\,s^{-1}\,m^{-3}$, and the nucleation rate in the photomechanical spallation regime observed in the atomistic simulations, $R \sim 10^{34}\,s^{-1}\,m^{-3}$. The corresponding threshold value of the nucleation free energy barrier can be estimated as $G_0^{th} \sim 23\,k_BT$.

The temperature dependence of surface tension of a liquid-vapor interface can be approximated as:

$$\sigma(T) = \sigma_0(1 - T/T_c)^\mu, \quad (4)$$

where σ_0 is a material dependent parameter, T_c is the critical temperature, and μ can be approximated as 1.26 based on the value of surface tension critical exponent obtained using the renormalization group technique [40]. The experimental values of the surface tension at the melting point and the corresponding temperature slops are available for a wide range of materials [41,42]. In the following analysis, the values of T_c, σ_0, and μ are directly calculated in atomistic MD simulations performed with Embedded Atom Method (EAM) potential parametrized for Al [43], Ni [44], Ag [45], and Cr [46] using the test area method [47] and are summarized in Table 1. The corresponding temperature dependencies of surface tension are plotted in Fig. 1. It should be noted that the obtained values of μ are lower than the theoretical prediction and depend on the interatomic potential, which can be attributed to the fact that the dependence given by Eq. (4) is derived for temperatures in the vicinity of the critical point [40], whereas the data provided in Fig. 1 is fitted for a broader temperature range.

Table 1
Parameters of Eq. (4) calculated for Al, Ni, Ag, and Cr described by EAM potentials.

	T_c [K]	σ_0 [J/m^2]	μ
Al	5800	0.910	1.07
Ni	9170	1.61	1.11
Ag	3380	0.573	1.19
Cr	6140	1.41	1.24

The analytically derived criterion for the onset of cavitation, Eq. (3), is tested and parametrized in a series of small-scale atomistic simulations performed for several cubic systems consisting of 4000 atoms and described by different interatomic potentials. In each simulation, the tensile pressure is kept at a constant level and the temperature is gradually increased with a heating rate of 1 K/ps. The onset of cavitation is identified by a rapid increase of the system volume. Fig. 2 illustrates the dependence of the cavitation threshold on temperature for Al, Ni, Ag, and Cr described by EAM potentials. The functional dependence given by Eq. (3) is able to describe the simulation results quite well with the proportionality coefficients α equal to 0.61, 0.66, 0.85, and 1.00 for Al, Ni, Ag, and Cr, respectively, which is close to the value of 0.7 obtained based on the theoretical consideration and the number of voids generated in large-scale atomistic simulations of spallation. The corresponding minimum free energy barriers for the onset of cavitation are 27.7, 25.5, 19.7, and 16.8 k_BT, for Al, Ni, Ag, and Cr model systems, respectively. These values of the free energy barrier are distributed around the value of 23 k_BT obtained through the rough order of magnitude estimation discussed above, and the deviation from the estimated value of the threshold pressure does not exceed 20% for all considered materials.

The nonsphericity of voids was checked in an attempt to explain the variability of α. Analysis of the results of a series of atomistic simulations has suggested that the surface area of voids exceeds the area of the corresponding spherical voids by 1.47, 1.70, 1.85, and 2.50 times for Al, Ag, Cr, and Ni, respectively. These values do not show direct correlation with the material dependence of the coefficient α, thus suggesting that this dependence cannot be explained by the difference in shapes of the voids alone.

Additionally, to evaluate the dependence of α on the size of the system used in the parametrization, the simulations of gradual 1 K/ps heating at constant tensile pressure were repeated for larger cubic systems consisting of 256,000 atoms. As can be seen from the results shown by red points and dashed lines in Fig. 2, temperature dependence of the cavitation threshold can be described well by Eq. (3), albeit with somewhat lower values of α (0.53, 0.52, 0.77, and 0.76 for Al, Ni, Ag, and Cr, respectively) and higher values of G_0^{th} (31.6, 32.2, 21.8, and 22.0 k_BT for Al, Ni, Ag, and Cr, respectively). The size dependence of α and G_0^{th} can be explained by the lower nucleation rate required for the onset of cavitation in a large system at the same rate of heating.

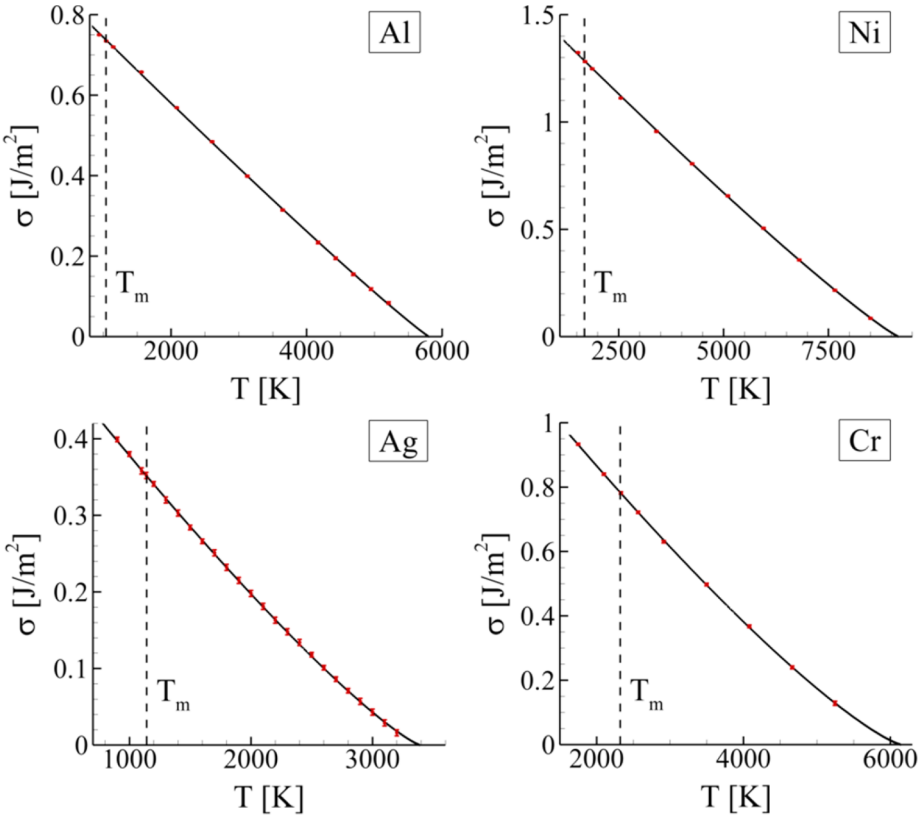

Fig. 1. Temperature dependence of surface tension calculated for Al, Ni, Ag, and Cr in a series of MD simulations (red symbols), and fitted to Eq. (4) (solid lines). The parameters of Eq. (4) obtained by the fitting are provided in Table 1. The error bars show standard deviation of the mean and are comparable with the size of the symbols. The values of equilibrium melting temperature calculated for the model materials described by EAM potentials are marked by vertical dashed lines.

3. Computational model for simulation of laser interactions with metals

To verify the applicability of the theoretical analysis discussed above, we perform a large-scale atomistic simulation of laser spallation of Ni target. The simulation is performed with a model combining the classical MD method with the two-temperature model (TTM) [22,24], which is shown to provide an accurate description of laser-induced processes at the atomic scale. The computational setup and parameters of the model are similar to those used in the simulations of laser-

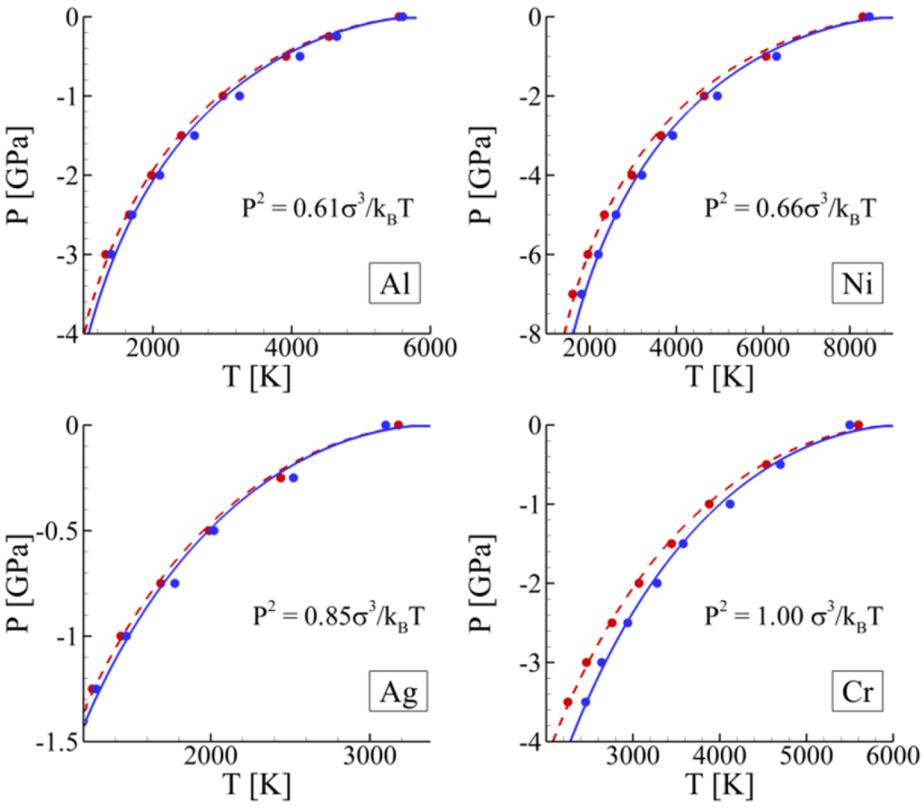

Fig. 2. Temperature and pressure dependence of the cavitation threshold predicted for Al, Ni, Ag, and Cr in a series of MD simulations of cubic systems consisting of 4000 atoms (blue points and solid lines) and 256,000 atoms (red points and dashed lines). The simulations are performed at constant values of tensile pressure and heating rates of 1 K/ps. The data points are fitted to the analytical dependence given by Eq. (3), and the corresponding functions obtained for the smaller systems are provided in the plot.

induced melting and resolidification reported in Ref. [15]. Briefly, the atomistic part of the TTM-MD model consists of 162 million atoms and represents the top 150 nm surface region of the target. In the lateral directions, parallel to the surface of the target, the dimensions of the computational systems are about 100 nm × 100 nm, and the periodic boundary conditions are applied. At the bottom of the atomistic part of the model, a pressure-transmitting, heat-conducting boundary condition is applied to ensure nonreflecting propagation of the laser-induced stress wave and heat transfer from the atomistic part of the computational system into the bulk of the target. The heat transfer into the bulk of the target is represented by conventional TTM equations solved down to a depth of 2.5 μm. The interatomic interactions between Ni atoms in the atomistic part of the model are described by the EAM potential parametrized by Mishin [44].

The applicability of the theoretical cavitation criterion for prediction of the maximum depth affected by the cavitation in a higher-fluence regime of phase explosion is verified using the results of a simulation of Al target irradiated by 100 fs laser pulse at 2000 J/m^2. A detailed discussion of this simulation and all computational parameters of the model are provided in Ref. [24].

4. Large-scale atomistic simulations of laser-induced cavitation

The process of laser-induced subsurface cavitation is investigated in a large-scale atomistic simulation of a Ni target irradiated by a 50 fs laser pulse at 1500 J/m^2, which is above the threshold for photomechanical spallation [23]. The temporal evolution of temperature and pressure in the irradiated target is illustrated in Fig. 3a and b. The fast laser energy deposition results in the generation of a strong pressure wave propagating from the surface to the bulk of the target, Fig. 3b. When the tensile component of the pressure wave passes through the molten part of the target, the free energy barrier for cavitation drops down to a minimum value of ~24.8 k_BT (Fig. 3d), which is below the cavitation threshold value of 25.5 k_BT identified in a series of small-scale atomistic simulations for Ni under well-controlled pressure and temperature conditions. This drop is sufficient to induce nucleation of multiple voids in the subsurface region of the target, at depth between 10 and 40 nm below the initial surface (see density contour plot in Fig. 3c and a snapshot of atomic configuration shown for a time of 100 ps in Fig. 3f). Both the time of the void nucleation and the spatial extent of the cavitation region are in a good quantitative agreement with the prediction of the theoretical model. Indeed, the region where the voids nucleate is the one where the temperature dependent threshold tensile pressure is exceeded and the free energy barrier for the cavitation drops below the threshold value (outlined by the purple dashed line in Fig. 3a–d). As one can see from Fig. 3c, the appearance of the cavitation region, which shows up as a green (low-density) region outlined by black dashed lines, can be traced back to the region identified by the theoretical criterion for the cavitation onset marked by the dashed pink line.

Note that the use of higher cavitation threshold predicted in simulations of gradual heating under tension performed for larger cubic systems containing 256,000 atoms (red dots and dashed lines in Fig. 2) leads to the overestimation of the size of the region affected by the cavitation. In particular, $G_0^{th} \sim 32.2\,k_BT$ obtained in the larger-scale simulations for Ni predicts the onset of cavitation in a region located

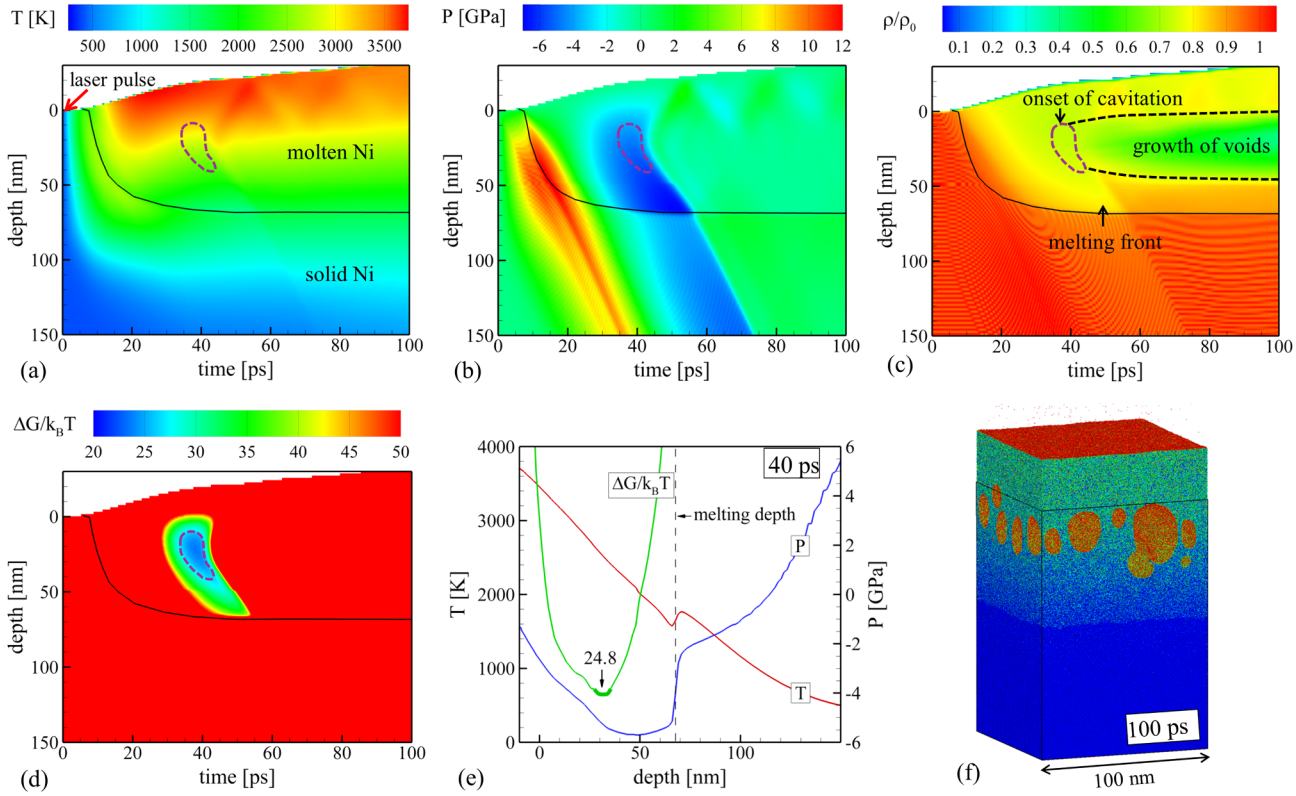

Fig. 3. (a–d) Contour plots of temporal and spatial evolution of temperature (a), pressure (b), density (c), and free energy barrier for the onset of cavitation (d) in a bulk Ni target irradiated by a 50 fs laser pulse at an absorbed laser fluence of 1500 J/m^2, which is just above the spallation threshold. The black solid lines show the location of the solid-liquid interface. Purple dashed lines outline the region with free energy barrier below 25.5 k_BT, where nucleation of voids is predicted theoretically and observed in the simulation. The region where the void growth is observed is outlined by black dashed lines in (c). (e) The spatial profile of lattice temperature (red), pressure (blue), and the free energy barrier (green) at the moment when the barrier reaches its minimum level. The scale of the free energy is from 20 to 50 k_BT, and a part of the curve for the free energy barrier below the threshold of *25.5* k_BT is shown by a thicker line. (f) An atomic configuration at a time of 100 ps, when the cavitation voids are clearly seen. The atoms are colored according to their potential energy, so that atoms in the solid part of the system are colored blue, atoms in the liquid phase are colored light blue to green, and atoms on free surfaces are colored orange and red.

between 10 and 60 nm below the original surface, which is wider than the actual zone of void nucleation observed in the simulation of laser spallation, Fig. 3c. As can be seen from Fig. 3a,b, the timescale of heating and tensile loading are both short, ~20 ps, whereas the heating from the melting temperature up to the threshold for the onset of cavitation takes, depending on the level of tensile pressure, from hundreds of picoseconds to nanoseconds. The use of the smaller system for model parametrization reduces the nucleation rate and compensates for the longer time of heating, thus yielding parameters more suitable for simulation of the ultrafast heating and mechanical loading conditions characteristic of femtosecond laser irradiation.

Following the nucleation, the voids grow, coalesce, and eventually percolate, leading to the separation/spallation of the top liquid layer from the bulk of the target. It is interesting to note that the depth where the free energy barrier reaches its minimum value, Fig. 3d, and the voids nucleate, Fig. 3c, does not coincide with the depth of the maximum tensile stresses are generated, Fig. 3b,e. In fact, the depth where the maximum tensile stresses are observed is below the region where the theoretical cavitation threshold is reached, and no void formation is observed at this depth. While the tensile stresses are increasing with depth and reach their maximum value close to the liquid-solid interface, the temperature decreases with the depth, leading to an increased ability of the material to support transient tensile stresses. The theoretical equation, Eq. (3), accounts for the interplay of these two factors and predicts the onset of the cavitation at an intermediate depth, where the free energy barrier reaches the sufficiently low values. This observation is consistent with the results of earlier MD simulations of photomechanical spallation of molecular targets [19,48], Ni [18,23], Cr [28,49], Al [24], and Ag [16,27].

The simple criterion defining the size of the cavitation region in laser spallation can also be used for evaluation of the maximum depth affected by cavitation at higher fluences, in the regime where the top layer of the target undergoes an explosive decomposition into vapor and small liquid droplets. While the magnitude of the tensile component of the laser-induced stress wave is reduced in this case by superposition with the compressive pressure wave generated by the phase explosion and ejection of material from the top layer [19,24], the tensile wave can still induce cavitation in a broad subsurface region. To illustrate the applicability of the cavitation criterion to this regime, we consider the results of an atomistic simulation reported in Ref. [24] for Al target irradiated by 100 fs laser pulse at 2000 J/m^2, above the threshold for the phase explosion. The evolution of free energy barrier for the onset of cavitation and the propagation of the melting front in this simulation can be seen from Fig. 4a. Following the laser excitation, the surface part of the target is rapidly heated and melted down to a depth of ~200 nm. Propagation of a tensile wave through the molten material creates conditions for void nucleation in a region extended down to a depth of ~110 nm. The appearance of voids is confirmed by visual analysis of a sequence of atomistic snapshots adapted from Ref. [24] and provided in Fig. 4b. In the snapshot shown for 50 ps, the voids are visible down to the depth of ~70 nm and are just starting to emerge in the underlying ~40-nm-thick layer. This observation is consistent with application of the theoretical criterion for the onset of cavitation. Similar to the analysis of the spallation regime illustrated by Fig. 3c, the black dashed line showing the maximum depth where the voids are observed in Fig. 4a originates from the region where the criterion for the cavitation onset is satisfied (outlined by the purple dashed line). During the following evolution, the voids grow and coalesce, leading to a gradual decomposition of the foamy liquid structure into individual liquid droplets, as can be seen from Fig. 4b.

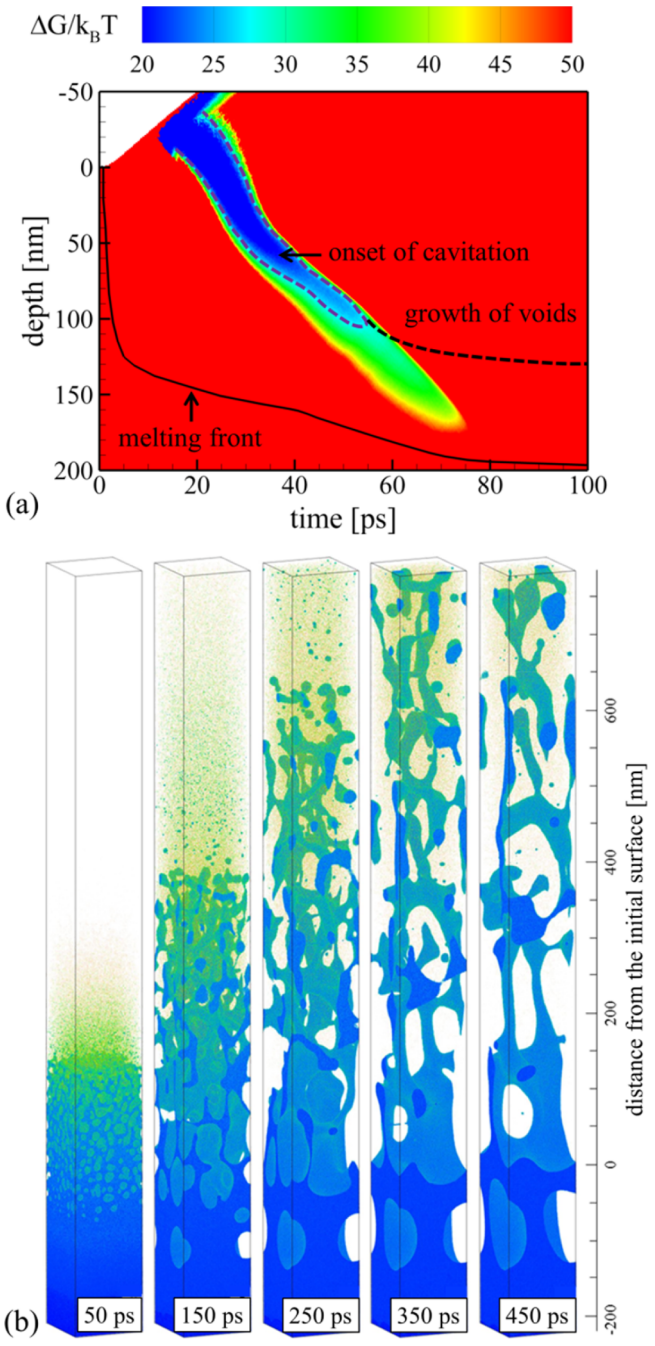

Fig. 4. (a) Contour plot of temporal and spatial evolution of free energy barrier for the onset of cavitation in an Al target irradiated by a 100 fs laser pulse at an absorbed laser fluence of 2000 J/m^2, which corresponds to the phase explosion regime. The black solid line shows the location of the solid-liquid interface. Purple dashed line outlines the region with free energy barrier below 27.7 k_BT, where nucleation of voids is predicted theoretically and observed in the simulation. The maximum depth where the voids are observed is marked by the black dashed line. (b) Atomic snapshots demonstrating nucleation and growth of voids. The atoms are colored according to their potential energy, with atoms in the solid and liquid phases are colored blue, while small clusters and vapor phase atoms are green and red. Fig. 4b is adapted from Ref. [24].

5. Summary

A criterion for the onset of cavitation in a molten metal is revisited, and a theoretical description of spallation is developed in terms of the free energy barrier for the onset of cavitation and void nucleation rate. The comparison of the number of voids generated in large scale atomistic simulations of short pulse laser ablation and the analytically evaluated nucleation rate has enabled formulation of the temperature-

pressure conditions in a region of an irradiated target affected by the cavitation, $P_{th}^2 = \alpha\sigma(T)^3/k_BT$. The analytical description is parametrized based on the results of atomistic simulations performed for Ni, Cr, Al, and Ag, and is shown to be applicable for a wide range of temperature and pressure conditions. While the value of parameter α exhibits some material dependence, the corresponding variation of the threshold pressure for the onset of cavitation is found to be less than 20% for all considered metals, and the value of 0.7 obtained analytically can be used for a reasonably accurate estimation of the spatial extent of the cavitation region. The results of large-scale atomistic simulations demonstrate the ability of the theoretical treatment to provide an adequate description of the onset of cavitation in both the spallation and phase explosion regimes. The cavitation criterion can be used to predict the onset of spallation in continuum-level models of laser-materials interaction.

CRediT authorship contribution statement

Maxim V. Shugaev: Conceptualization, Investigation, Writing - original draft. **Leonid V. Zhigilei:** Writing - review & editing, Supervision.

Acknowledgements

Financial support for this work was provided by the National Science Foundation (NSF) through Grant No. DMR-1610936. Computational support was provided by the Oak Ridge Leadership Computing Facility (INCITE project MAT130) and NSF through the Extreme Science and Engineering Discovery Environment (Project No. TG-DMR110090).

References

[1] B.N. Chichkov, C. Momma, S. Nolte, F. von Alvensleben, A. Tünnermann, Femtosecond, picosecond and nanosecond laser ablation of solids, Appl. Phys. A 63 (1996) 109–115.
[2] R. Le Harzic, N. Huot, E. Audouard, C. Jonin, P. Laporte, S. Valette, A. Fraczkiewicz, R. Fortunier, Comparison of heat-affected zones due to nanosecond and femtosecond laser pulses using transmission electronic microscopy, Appl. Phys. Lett. 80 (2002) 3886–3888.
[3] A.Y. Vorobyev, C. Guo, Effects of nanostructure-covered femtosecond laser-induced periodic surface structures on optical absorptance of metals, Appl. Phys. A 86 (2007) 321–324.
[4] S. Barcikowski, A. Hahn, A.V. Kabashin, B.N. Chichkov, Properties of nanoparticles generated during femtosecond laser machining in air and water, Appl. Phys. A 87 (2007) 47–55.
[5] N. Haustrup, G.M. O'Connor, Impact of wavelength dependent thermo-elastic laser ablation mechanism on the generation of nanoparticles from thin gold films, Appl. Phys. Lett. 101 (2012) 263107.
[6] A. Miotello, N. Patel, Pulsed laser deposition of cluster-assembled films for catalysis and the photocatalysis relevant to energy and the environment, Appl. Surf. Sci. 278 (2013) 19–25.
[7] Q.-Z. Zhao, S. Malzer, L.-J. Wang, Self-organized tungsten nanospikes grown on subwavelength ripples induced by femtosecond laser pulses, Opt. Express 15 (2007) 15741–15746.
[8] Y. Dai, M. He, H. Bian, B. Lu, X. Yan, G. Ma, Femtosecond laser nanostructuring of silver film, Appl. Phys. A 106 (2012) 567–574.
[9] A.Y. Vorobyev, C. Guo, Enhanced absorptance of gold following multipulse femtosecond laser ablation, Phys. Rev. B 72 (2005) 195422.
[10] J. Vincenc Oboňa, V. Ocelík, J.C. Rao, J.Z.P. Skolski, G.R.B.E. Römer, A.J. Huis in 't Veld, J.T.M.D. Hosson, Modification of Cu surface with picosecond laser pulses, Appl. Surf. Sci. 303 (2014) 118–124.
[11] C.J. Lin, F. Spaepen, Nickel-niobium alloys obtained by picosecond pulsed laser quenching, Acta Metall. 34 (1986) 1367–1375.
[12] A. Vailionis, E.G. Gamaly, V. Mizeikis, W. Yang, A.V. Rode, S. Juodkazis, Evidence of superdense aluminium synthesized by ultrafast microexplosion, Nat. Commun. 2 (2011) 445.
[13] C. Wu, D.A. Thomas, Z. Lin, L.V. Zhigilei, Runaway lattice-mismatched interface in an atomistic simulation of femtosecond laser irradiation of Ag film–Cu substrate system, Appl. Phys. A 104 (2011) 781–792.
[14] M.V. Shugaev, C.-Y. Shih, E.T. Karim, C. Wu, L.V. Zhigilei, Generation of nanocrystalline surface layer in short pulse laser processing of metal targets under conditions of spatial confinement by solid or liquid overlayer, Appl. Surf. Sci. 417 (2017) 54–63.
[15] X. Sedao, M.V. Shugaev, C. Wu, T. Douillard, C. Esnouf, C. Maurice, S. Reynaud, F. Pigeon, F. Garrelie, L.V. Zhigilei, J.-P. Colombier, Growth twinning and generation of high-frequency surface nanostructures in ultrafast laser-induced transient melting and resolidification, ACS Nano 10 (2016) 6995–7007.
[16] C. Wu, M.S. Christensen, J.-M. Savolainen, P. Balling, L.V. Zhigilei, Generation of subsurface voids and a nanocrystalline surface layer in femtosecond laser irradiation of a single-crystal Ag target, Phys. Rev. B 91 (2015) 035413.
[17] G. Paltauf, P.E. Dyer, Photomechanical processes and effects in ablation, Chem. Rev. 103 (2003) 487–518.
[18] E. Leveugle, D.S. Ivanov, L.V. Zhigilei, Photomechanical spallation of molecular and metal targets: molecular dynamics study, Appl. Phys. A 79 (2004) 1643–1655.
[19] L.V. Zhigilei, B.J. Garrison, Microscopic mechanisms of laser ablation of organic solids in the thermal and stress confinement irradiation regimes, J. Appl. Phys. 88 (2000) 1281–1298.
[20] J.-M. Savolainen, M.S. Christensen, P. Balling, Material swelling as the first step in the ablation of metals by ultrashort laser pulses, Phys. Rev. B 84 (2011) 193410.
[21] X. Sedao, A. Abou Saleh, A. Rudenko, T. Douillard, C. Esnouf, S. Reynaud, C. Maurice, F. Pigeon, F. Garrelie, J.-P. Colombier, Self-arranged periodic nanovoids by ultrafast laser-induced near-field enhancement, ACS Photonics 5 (2018) 1418–1426.
[22] D.S. Ivanov, L.V. Zhigilei, Combined atomistic-continuum modeling of short-pulse laser melting and disintegration of metal films, Phys. Rev. B 68 (2003) 064114.
[23] L.V. Zhigilei, Z. Lin, D.S. Ivanov, Atomistic modeling of short pulse laser ablation of metals: connections between melting, spallation, and phase explosion, J. Phys. Chem. C 113 (2009) 11892–11906.
[24] C. Wu, L.V. Zhigilei, Microscopic mechanisms of laser spallation and ablation of metal targets from large-scale molecular dynamics simulations, Appl. Phys. A 114 (2014) 11–32.
[25] A.K. Upadhyay, N.A. Inogamov, B. Rethfeld, H.M. Urbassek, Ablation by ultrashort laser pulses: atomistic and thermodynamic analysis of the processes at the ablation threshold, Phys. Rev. B 78 (2008) 045437.
[26] C.-Y. Shih, M.V. Shugaev, C. Wu, L.V. Zhigilei, Generation of subsurface voids, incubation effect, and formation of nanoparticles in short pulse laser interactions with bulk metal targets in liquid: molecular dynamics study, J. Phys. Chem. C 121 (2017) 16549–16567.
[27] C. Wu, L.V. Zhigilei, Nanocrystalline and polyicosahedral structure of a nanospike generated on metal surface irradiated by a single femtosecond laser pulse, J. Phys. Chem. C 120 (2016) 4438–4447.
[28] A. Abou-Saleh, E.T. Karim, C. Maurice, S. Reynaud, F. Pigeon, F. Garrelie, L.V. Zhigilei, J.P. Colombier, Spallation-induced roughness promoting high spatial frequency nanostructure formation on Cr, Appl. Phys. A 124 (2018) 308.
[29] S.V. Starikov, V.V. Pisarev, Atomistic simulation of laser-pulse surface modification: predictions of models with various length and time scales, J. Appl. Phys. 117 (2015) 135901.
[30] M.E. Povarnitsyn, K.V. Khishchenko, P.R. Levashov, Phase transitions in femtosecond laser ablation, Appl. Surf. Sci. 255 (2009) 5120–5124.
[31] D.E. Grady, The spall strength of condensed matter, J. Mech. Phys. Solids 36 (1988) 353–384.
[32] Q. An, G. Garrett, K. Samwer, Y. Liu, S.V. Zybin, S.-N. Luo, M.D. Demetriou, W.L. Johnson, W.A. Goddard, Atomistic characterization of stochastic cavitation of a binary metallic liquid under negative pressure, J. Phys. Chem. Lett. 2 (2011) 1320–1323.
[33] T.T. Bazhirov, G.E. Norman, V.V. Stegailov, Cavitation in liquid metals under negative pressures. Molecular dynamics modeling and simulation, J. Phys. Condens. Matter 20 (2008) 114113.
[34] A.V. Neimark, A. Vishnyakov, The birth of a bubble: a molecular simulation study, J. Chem. Phys. 122 (2005) 054707.
[35] T. Kinjo, M. Matsumoto, Cavitation processes and negative pressure, Fluid Ph. Equilibria 144 (1998) 343–350.
[36] D. Turnbull, J.C. Fisher, Rate of nucleation in condensed systems, J. Chem. Phys. 17 (1949) 71–73.
[37] H. Okumura, N. Ito, Nonequilibrium molecular dynamics simulations of a bubble, Phys. Rev. E 67 (2003) 045301.
[38] A.Y. Kuksin, G.E. Norman, V.V. Pisarev, V.V. Stegailov, A.V. Yanilkin, Theory and molecular dynamics modeling of spall fracture in liquids, Phys. Rev. B 82 (2010) 174101.
[39] E. Dekel, S. Eliezer, Z. Henis, E. Moshe, A. Ludmirsky, I.B. Goldberg, Spallation model for the high strain rates range, J. Appl. Phys. 84 (1998) 4851–4858.
[40] N. Goldenfeld, Lectures on Phase Transitions and the Renormalization Group, Addison-Wesley, Advanced Book Program, Reading, Mass., 1992.
[41] I. Egry, E. Ricci, R. Novakovic, S. Ozawa, Surface tension of liquid metals and alloys — recent developments, Adv. Colloid Interface Sci. 159 (2010) 198–212.
[42] H.M. Lu, Q. Jiang, Surface tension and its temperature coefficient for liquid metals, J. Phys. Chem. B 109 (2005) 15463–15468.

[43] Y. Mishin, D. Farkas, M.J. Mehl, D.A. Papaconstantopoulos, Interatomic potentials for monoatomic metals from experimental data and ab initio calculations, Phys. Rev. B 59 (1999) 3393–3407.
[44] Y. Mishin, Atomistic modeling of the γ and γ′-phases of the Ni–Al system, Acta Mater. 52 (2004) 1451–1467.
[45] S.M. Foiles, M.I. Baskes, M.S. Daw, Embedded-atom-method functions for the fcc metals Cu, Ag, Au, Ni, Pd, Pt, and their alloys, Phys. Rev. B 33 (1986) 7983–7991.
[46] Z. Lin, R.A. Johnson, L.V. Zhigilei, Computational study of the generation of crystal defects in a bcc metal target irradiated by short laser pulses, Phys. Rev. B 77 (2008) 214108.
[47] G.J. Gloor, G. Jackson, F.J. Blas, E. de Miguel, Test-area simulation method for the direct determination of the interfacial tension of systems with continuous or discontinuous potentials, J. Chem. Phys. 123 (2005) 134703.
[48] E. Leveugle, L.V. Zhigilei, Microscopic mechanisms of short pulse laser spallation of molecular solids, Appl. Phys. A 79 (2004) 753–756.
[49] E.T. Karim, Z. Lin, L.V. Zhigilei, Molecular dynamics study of femtosecond laser interactions with Cr targets, AIP Conf. Proc. 1464 (2012) 280–293.